JOURNAL OF MATERIALS SCIENCE 31 (1996) 2149–2157

Inertia-friction welding of SiC-reinforced 8009 aluminium

T. J. LIENERT, W. A. BAESLACK III*, J. RINGNALDA and H. L. FRASER
*Department of Materials Science and Engineering and *College of Engineering*
The Ohio State University, Columbus, OH 43210 USA

Inertia-drive friction welding (IFRW) of an 8009 Al alloy (Al–8.5 Fe–1.7 Si–1.3 V, wt %) reinforced with 11 volume per cent SiC particles (8009/SiC/11$_p$) has been investigated. Inertia-drive friction welds were made with constant energy at two levels of axial force. The microstructures of the base material and the welds were characterized using optical and scanning electron microscopy, while the mechanical properties were evaluated using microhardness and tensile testing. Examination of weld sections revealed that the hot deformation experienced during welding produced a homogenized microstructure with a uniform distribution of SiC particles along the bond line. No evidence of a chemical reaction between the SiC and the matrix was found in any of the welds, but cracking of some of the larger SiC particles was observed in the base material as well as in the IFR welds. The average microhardness of the various heat-and-deformation affected zones (HDZs) of the welds did not vary greatly from that of the base material, and no weld induced weak regions were discerned. The room-temperature (RT) tensile strength of the IFR welds exceeded 90 per cent of the base material. The weld tensile specimens failed at the outer edge of the HDZ for all of the welds tested. The fracture surface of the 8009 matrix of tensile samples for both the base material and the welds exhibited a dimpled appearance indicating a ductile failure, while fracture through the SiC appeared to occur in a brittle fashion. IFRW has proven effective in joining 8009/SiC/11$_p$ with little loss in RT hardness and tensile properties.

1. Introduction

High-temperature discontinuously-reinforced aluminium (HTDRA) composites are a relatively new class of aerospace material targeted for structural applications in the range of temperatures between 150–370 °C [1]. Allied Signal Inc. (Morristown, NJ) has recently introduced an 8009/SiC/11$_p$* HTDRA composite manufactured using rapid solidification/powder metallurgy (RS/PM) techniques [3]. Potential applications for 8009/SiC/11$_p$ include aircraft wing skins, missile bodies, and other aerospace structures that are heated aerodynamically or that reside in close proximity to the engines.

The 8009 aluminium alloy matrix (Al–8.5 Fe–1.7 Si–1.3 V, wt %) is strengthened by a fine distribution of nearly spherical $Al_{13}(Fe,V)_3Si$ (Im3 structure) intermetallic dispersoids (~ 0.5 nm in size) formed during the RS process and subsequent consolidation/thermomechanical processing (TMP) operations. These dispersoids are stable to temperatures approaching 370 °C and have very low coarsening rates at working temperatures. The fine dispersoids, as well as a small alpha-aluminium grain size (0.5–2.0 μm) resulting from RS processing, give the 8009 alloy superior high temperature mechanical properties relative to conventional Al alloys [4, 5]. The addition of 11 volume percent SiC particles (SiC_p) to the 8009 matrix alloy results in a metal–matrix composite (MMC) with increased specific strength and stiffness [1, 3].

The effective use of 8009/SiC/11$_p$ will often depend upon its ability to be joined both to itself and to dissimilar materials. Since the properties of this composite derive from its unique microstructure, welding processes must be chosen that limit coarsening or dissolution of the $Al_{13}(Fe,V)_3Si$ dispersoids [6, 7] and avoid chemical reactions between the SiC particles and the matrix [8]. One potential approach to joining this material involves the use of a solid-state process such as friction welding (FRW).

Friction welding is a solid-state welding process in which heat is generated by friction from the relative motion of the parts to be welded [9, 10]. The heat of welding originates from direct conversion of the mechanical energy of the moving part to thermal energy

* Aluminium metal–matrix composites (Al-MMCs) are normally specified according to a five part nomenclature developed by the Aluminium Association (AA) and later adopted by the American National Standards Institute (ANSI) [2]. In this specification, the matrix alloy is listed first, followed sequentially by the reinforcement material, and the volume percent and shape of reinforcement, each separated by a slash. The heat-treatment designation, where appropriate, is placed after the percent and shape of reinforcement. For example, 8009/SiC/11$_p$ refers to an AA 8009 alloy matrix containing 11 volume percent SiC particles.

0022–2461

and strain energy. The application of an axial force maintains intimate contact of the parts and causes plastic deformation of the material near the interface during welding. More than 90% of the energy consumed in plastic deformation is transformed into heat, although a small fraction of the energy is stored in the material as strain energy [11]. Deformation is largely restricted to the volume of material adjacent to the original interfaces by an adiabatic shear process [12, 13]. During adiabatic shearing, the temperature rise in this volume results in a local loss in flow stress thereby decreasing the resistance of the material to further deformation. As a result of the lowered resistance, deformation tends to be localized in this volume, and the process continues in a self-propagating fashion.

There are two major process variations for FRW: continuous-drive welding and inertia-drive welding [14]. The distinction between the two variations lies in the method of energy delivery to the weld. In continuous-drive FRW, the moving part is continuously driven by a motor at a constant speed. A brake is applied to terminate the process after a preset time. Inertia-FRW (IFRW) employs the stored energy of a decelerating flywheel to effect the weld. The thermal cycle for inertia-drive welds is typically much shorter (~ 1 s) than that for direct-drive welds (~ 20 s) [9]. The rapid thermal cycle associated with IFRW is particularly well suited for 8009/SiC/11$_p$.

IFRW has been employed to successfully join several high-temperature Al–Fe alloys strengthened by intermetallic dispersoids [6, 7, 15, 16], as well as MMCs with conventional Al alloy matrices [17–21] and oxide-dispersion strengthened (ODS) materials [22, 23]. The purpose of this study was to produce and characterize IFR welds in an 8009/SiC/11$_p$ HTDRA composite.

2. Experimental procedure

A 9 cm diameter experimental extrusion of 8009/SiC/11$_p$ material was supplied by Allied Signal Inc. The powder for the 8009 matrix was produced by mechanically comminuting planar flow cast (PFC) ribbons to -40 mesh. A kinetic blending process was employed to disperse and bond the SiC$_p$ in the 8009 alloy matrix powder. Billets of the composite powder were vacuum hot-pressed and subsequently extruded to size at temperatures well below the solidus temperature of the 8009 alloy [3].

Cylindrical samples, 2.54 cm in diameter and 6.3 cm in length, were machined from the extrusion (with the 6.3 cm dimension parallel to the extrusion direction) using polycrystalline diamond tooling. Joining was performed with an MTI model 120 inertia-welding system. The welding parameters were identical to those used in previous work on monolithic Al–Fe–Si–V alloys except that higher axial forces were used for the 8009/SiC/11$_p$ composite [6, 7]. The samples were IFR welded at 5000 rpm (524 rad s^{-1}) and an initial flywheel kinetic energy of 22.9 kJ. Welds were made at two different levels of axial force: 111.6 kN and 156.2 kN. Welding time for both levels of axial force was less than two seconds. The welds made at 111.6 kN will be hereafter referred to as the low axial force (LAF) welds, while the welds made at 156.2 kN will be referred to as the high axial force (HAF) welds.

After welding, randomly selected samples were sectioned longitudinally (i.e. parallel to the extrusion direction) using electrical discharge machining (EDM) equipment with a traveling wire. One half of each specimen was used for microstructural characterization, whilst the other half was used for mechanical testing. Metallographic specimens were prepared from each weld using standard practice through 1 μm diamond polishing. Final polishing was performed using a colloidal silica suspension. After polishing, various locations across the welds were examined using optical microscopy at magnifications up to 1000×. The specimens for optical microscopy were etched for various times using a Keller's etch. Selected specimens were examined as-polished using a scanning-electron microscope (SEM) operated in secondary and back-scattered-electron modes.

Knoop microhardness traverses extending from the centre of the weld to the unaffected base material were made along the specimen axial centreline and outer periphery. Microhardness testing was performed with a load of 200 g and a dwell time of 15 s. Subscale tensile specimens measuring 7.1 cm in length and 0.23 cm in thickness, with a 2.54 cm gauge length, were machined from the second half of the weld specimens, as well as from the base material. Tensile testing was performed at room temperature on an Instron 1331 test frame at a strain rate of 1×10^{-4} sec^{-1}. The strain during tensile testing was measured by attaching an extensometer on the sample. The fracture surfaces of the tensile specimens were examined using an SEM.

3. Results and discussion

3.1. Microstructural analysis

3.1.1. Base material

Optical and SEM micrographs of the 8009/SiC/11$_p$ base material are shown in Fig. 1(a,b) and Fig. 1(c,d) respectively. Individual bands of consolidated particles of the RS ribbon were discernible. The bands of the base material were polycrystalline and exhibited a high aspect ratio (> 20 to 1) as a consequence of extrusion processing. Contrast in the optical micrographs appeared to result from variations in the density and size of the $Al_{13}(Fe,V)_3Si$ dispersoids, as well as differences in ribbon orientation with respect to the sectioning plane. The variations in the density and size of the $Al_{13}(Fe,V)_3Si$ dispersoids likely occurred due to variations in processing [24]. Small featureless areas were also evident in the base material. SEM examination revealed that the featureless areas are rich in Al and do not appear to have been rapidly solidified. They may be remnants of the kinetic blending process which were collected with the RS ribbons and remained in the final product [25].

The base material microstructure was characterized by a non-uniform distribution of SiC particles. Some

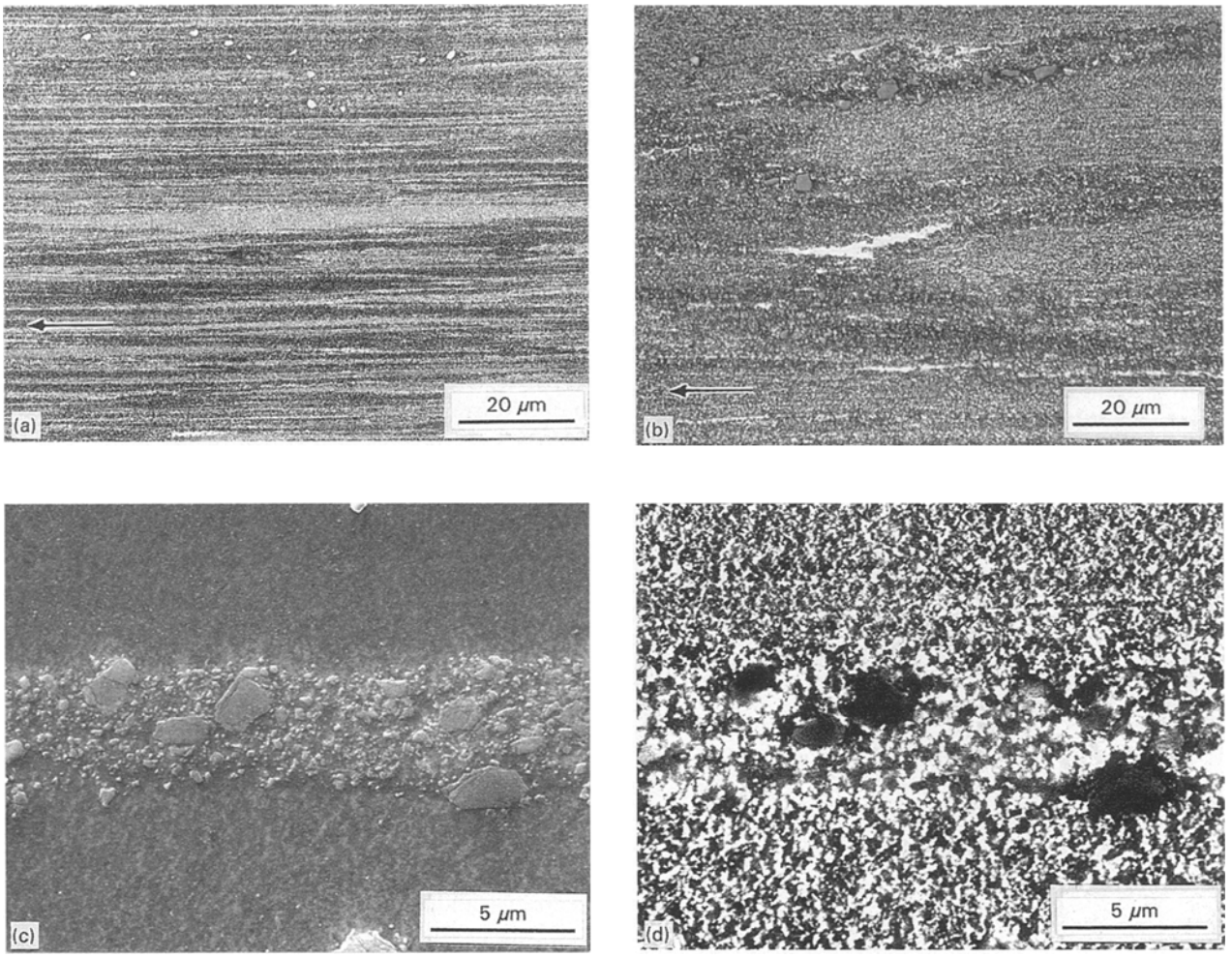

Figure 1 Micrographs of 8009/SiC/11$_p$ extruded base material: (a, b) optical micrographs; (c) SEM micrograph in SE mode; (d) SEM micrograph in BSE mode. Arrows in (a) and (b) indicate extrusion direction.

areas contained a high density of SiC, while adjacent areas were nearly devoid of SiC. The inhomogeneous distribution of SiC was likely due to insufficient kinetic blending during production. The majority of the SiC particles were approximately 0.5–3 μm in size, although particles up to 10 μm were observed. Some of the larger SiC particles appeared to be cracked.

Scanning electron microscopy (SEM) allows examination of some features of the microstructure not discernible with optical microscopy. The micrograph in Fig. 1c was taken using the secondary electron (SE) mode, while the micrograph in Fig. 1d was taken using the backscattered electron (BSE) mode. Contrast in the BSE imaging mode is a strong function of composition with constituents or phases containing heavier elements appearing lighter. The alpha-aluminium matrix appeared medium grey in the SE mode and nearly black in the BSE mode, while the SiC particles showed up dark grey in the SE mode and black in the BSE mode (the white around the edges of some of the SiC particles in SE photograph is probably caused by charging effects). In addition, a light grey minor phase was visible in the SE mode. The same phase appeared white in the BSE mode. This observation suggests that this phase is likely a distribution of the $Al_{13}(Fe,V)_3Si$ dispersoids discussed earlier. The presence of relatively heavy elements Fe and V increased the backscattering coefficient of the dispersoids relative to the Al matrix. Consequently, the dispersoids looked white in the BSE mode and were more easily discerned. Note that the dispersoid size and distribution varied somewhat with location.

3.1.2. Weld zone

No defects were observed in any of the weld zones. As shown in Fig. 2, a symmetrically uniform flash or upset was formed around the circumference of each sample during welding. The extent of the upset for the HAF welds was larger than for the LAF welds. The average axial displacement after welding was approximately 0.4 cm for the LAF welds and 0.9 cm for the HAF welds.

Optical macrographs of the weld areas of the LAF and HAF welds are presented in Fig. 3(a,b). Two distinct regions of the weld heat- and deformation-affected zone (HDZ) were evident. A distinct inner HDZ (IHDZ) was visible along the bond line. The IHDZ represents the volume of material in which deformation is concentrated during adiabatic shearing, as discussed earlier. The shape of the IHDZs of the welds resembled a slender figure-eight. The IHDZs were narrow at the weld centreline and near the periphery, and wider in between. The widest part of the IHDZs was located at a radial distance of 2/3–3/4 of the sample radius from the axial centreline. An outer

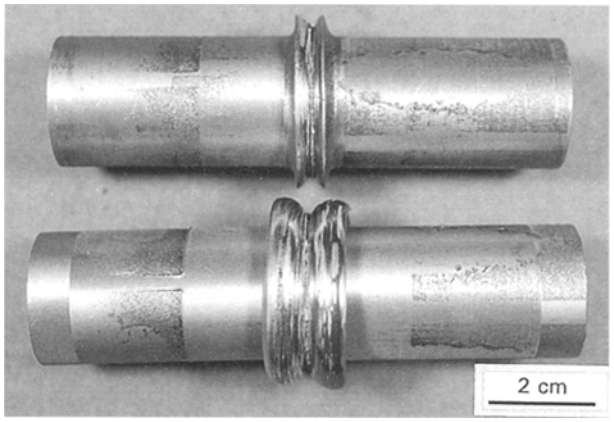

Figure 2 Inertia-friction welds produced using low axial force (top) and high axial force (bottom).

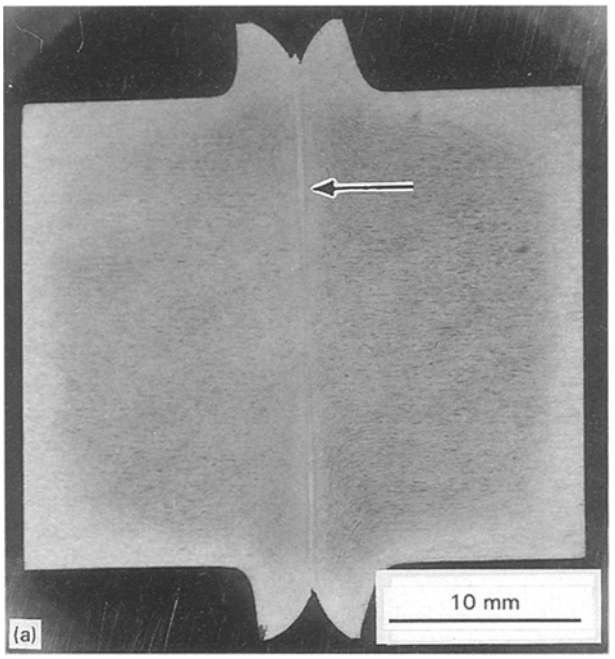

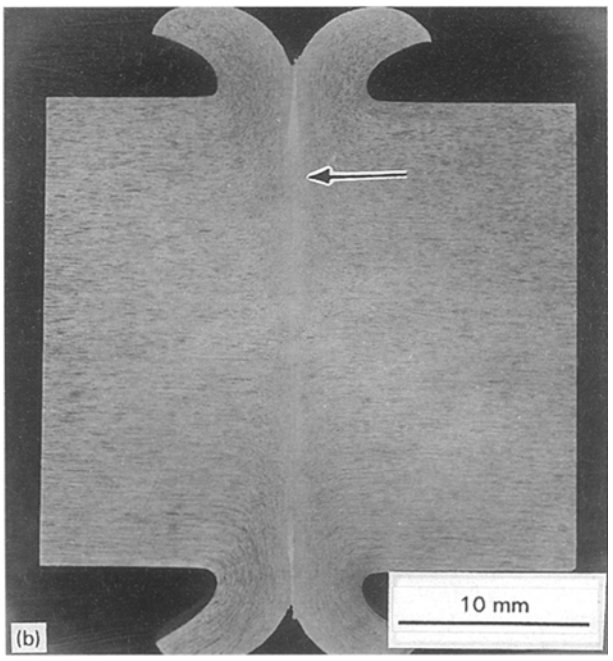

Figure 3 Optical micrograph of (a) LAF weld and (b) HAF weld. Arrows indicate bond line.

HDZ (OHDZ) of deformed bands of the base material was also discernible. The OHDZ of the welds widened with increasing radial distance from the axial centreline. The variation in shape of the HDZ in inertia-friction welds results from variations in both input power [9, 10] and unit pressure [26] distributions as functions of time and radial distance.

Optical micrographs of a longitudinal section of the HDZ of a HAF weld are shown in Fig. 4(a,b). The IHDZ of the welds exhibited a homogeneous microstructure with a relatively uniform distribution of SiC and $Al_{13}(Fe,V)_3Si$ dispersoids resulting from the extensive deformation and mechanical mixing experienced during welding. Individual bands in the RS matrix were no longer distinguishable in the IHDZ. The outer HDZ (OHDZ) of the welds experienced less deformation and mixing, and individual bands were still readily discernible. The bands at the outer edge of the OHDZ displayed a much smaller aspect ratio than those of the base material as a result of the shear deformation experienced locally during welding. In fact, many of the bands at the outer edge of the OHDZ appeared almost equiaxed. Structures similar to those discussed above for the HAF welds were also observed in the HDZs of the LAF welds.

The IHDZ for the HAF welds varied in width from approximately 50 μm at the axial centreline to about 600 μm at a position near the 3/4 radius. The total width of the OHDZ was approximately 100 μm at the centreline and 8 mm near the periphery. Note that the orientation of the different bands in the HDZ was changed relative to that in the base material by plastic flow during joining. In this cross-section, the elongated bands of the base material near the weld interface have been deformed and turned radially. In three dimensions, the bands were actually deformed in a spiral fashion with components of flow in the axial, radial and circumferential directions. The width of the IHDZs of the LAF welds varied from about 50 μm at the axial centreline to approximately 250 μm near the 3/4 radius position. The OHDZs of the LAF welds widened from about 60 μm near the centreline to approximately 8mm near the periphery.

Observations made using optical microscopy were confirmed by SEM. Fig. 5a is an SEM micrograph of the outer HDZ of a HAF weld, while Fig. 5(b,c) are SEM micrographs of the inner HDZ of the same weld. No evidence of a chemical reaction between the SiC and the matrix was observed in any of the metallographic sections. The SiC and $Al_{13}(Fe,V)_3Si$ dispersoids were distributed uniformly throughout the IHDZ. Some of the larger SiC particles in the HDZ appeared cracked. Crushing of reinforcement particles during deformation of MMCs at high strains has been reported by several researchers and was not unexpected in these IFR welds [27–29]. It is not clear, however, if these particles cracked during production of the composite or during IFRW. Similar observations were made during SEM examination of the LAF welds.

Featureless (white) areas were occasionally observed near the weld periphery in the IHDZ of the welds, especially the LAF welds. Fig. 6 is an optical

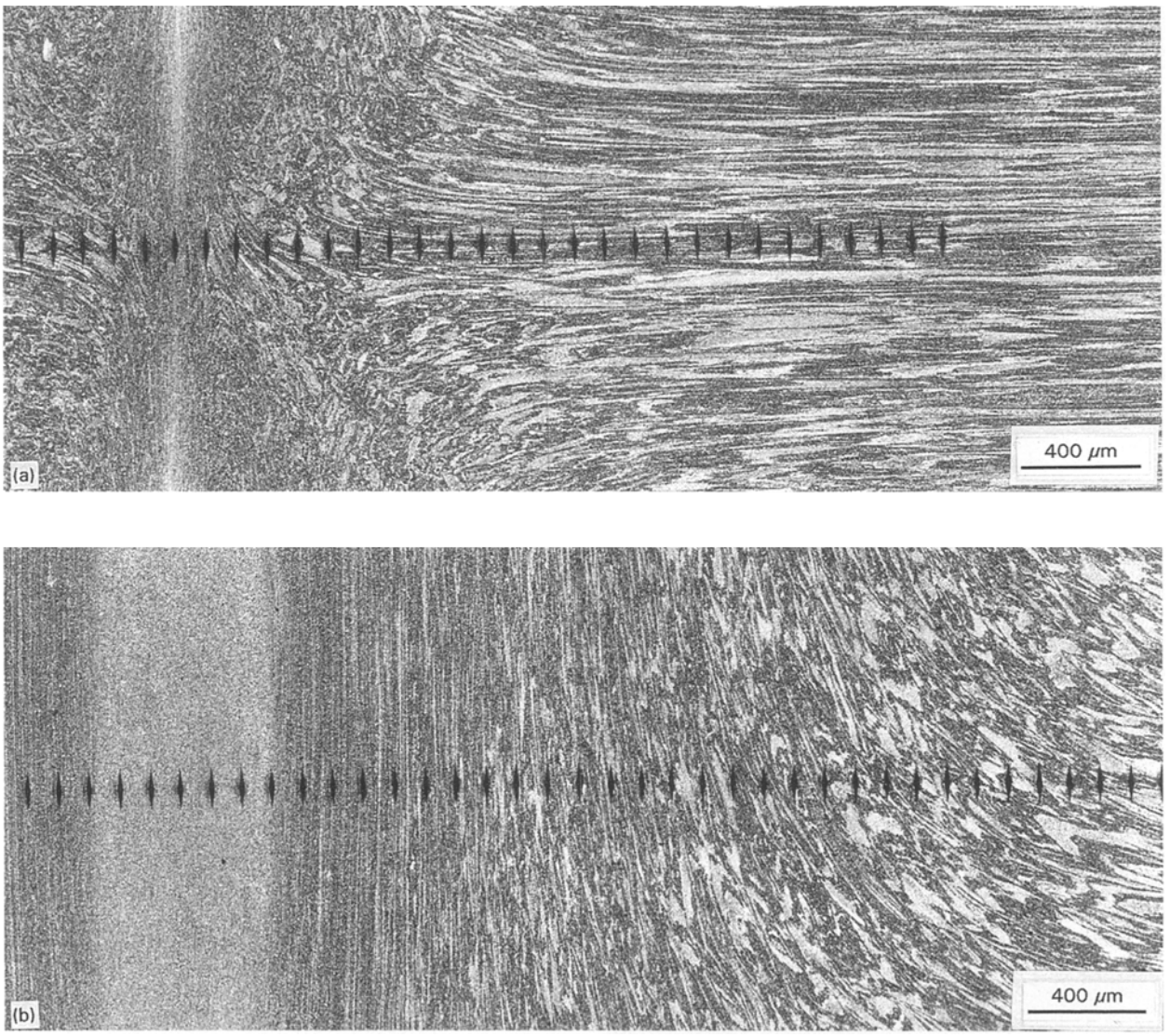

Figure 4 High axial force weld: (a, b) optical micrographs near the axial centreline and near the periphery, respectively.

micrograph of the IHDZ near the periphery of a LAF weld. In this section, the featureless regions were needle shaped and were several hundred microns long and approximately 30 microns wide. The long dimension of the needles was oriented parallel to the original joint interfaces. Regions of dark contrast were often observed adjacent to the featureless regions. Similar features have been reported in IFR welds on monolithic Al–Fe–Si–V alloys, as well as other Al–Fe alloys [6, 7, 15]. Bright field imaging of similar featureless areas in IFR welds on monolithic RS/PM Al–Fe–Si–V alloys using TEM revealed a region with large α-aluminium grain size and a very low density of $Al_{13}(Fe,V)_3Si$ dispersoids adjacent to areas with coarsened $Al_{13}(Fe,V)_3Si$ dispersoids [6, 7].

The origin of the featureless streaks is not well understood and is still under investigation. Several theories have been put forth to explain their existence. The first theory maintains that the featureless regions resulted from localized, nonuniform deformation in the HDZ [6, 7]. The dispersoid lean regions in IFR welds of monolithic Al–Fe–Si–V alloys are thought to arise from high shear and compressive stresses that locally extrude alpha-aluminium regions with a low density of $Al_{13}(Fe,V)_3Si$ dispersoids from the base metal [6, 7]. The lack of dispersoids in these regions accounts for its light contrast in optical micrographs and its low microhardness.

The second theory involves the formation of liquid in the IHDZ. The featureless phase may be the remnant of a thin liquid layer that formed late in the welding process. The absence of a solidification structure in the featureless phase in this case would not be surprising since considerable recovery and recrystallization of the IHDZ would be expected to occur during the last phase of welding and during cooling.

While the formation of thick liquid films that extend over large areas during FRW is unlikely, the formation of thin liquid layers along grain boundaries is possible. Evidence of partial melting during FRW has been reported by several researchers. Results of modeling by Cheng using the finite difference method suggested that melting can occur near the weld interface during IFRW of steels [30]. Midling and Grong proposed that partial melting of the IHDZ occurs during direct-drive FRW of Al alloys and Al/SiC composites producing thixotropic deformation behaviour as a result of the very high local strain rates [20]. Formation of liquid can occur at temperatures well below the bulk liquidus temperature. Tensi *et al.* have

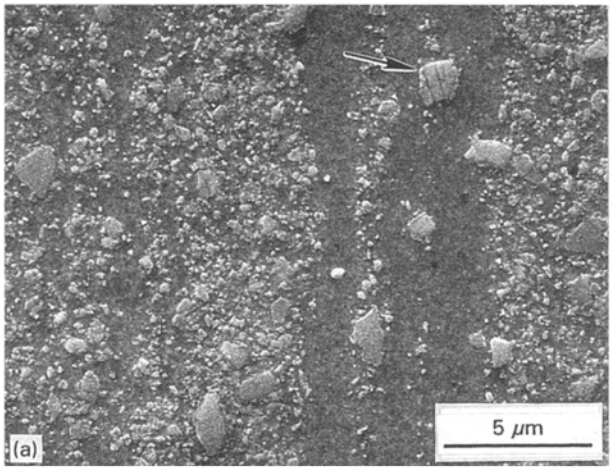

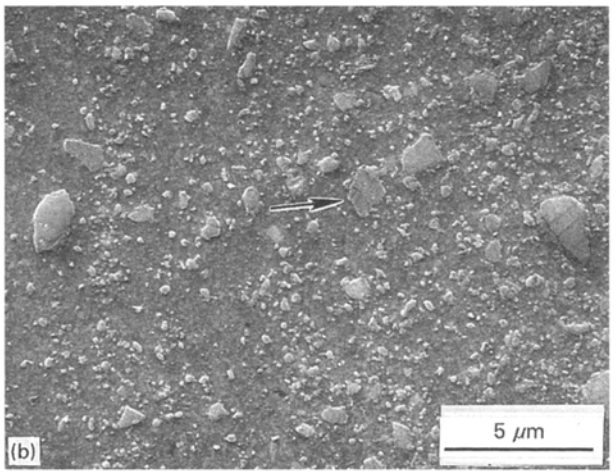

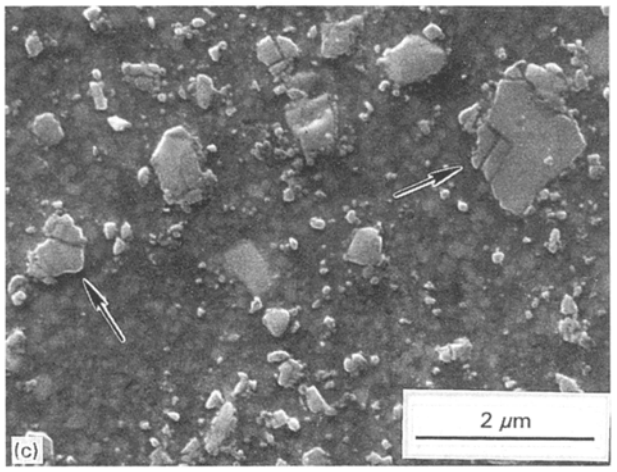

Figure 5 SEM micrographs of a HAF weld: (a) OHDZ; (b, c) IHDZ. Arrows indicate cracked SiC particles.

measured peak temperatures near the weld interface equal to the solidus temperatures of several Al alloys during direct-drive FRW [31]. Moreover, they observed microstructural evidence of partial melting in the form of widened grain boundaries.

3.2. Mechanical properties

3.2.1. Microhardness testing

The Knoop microhardness of the base material varied considerably due to its non-uniform microstructure.

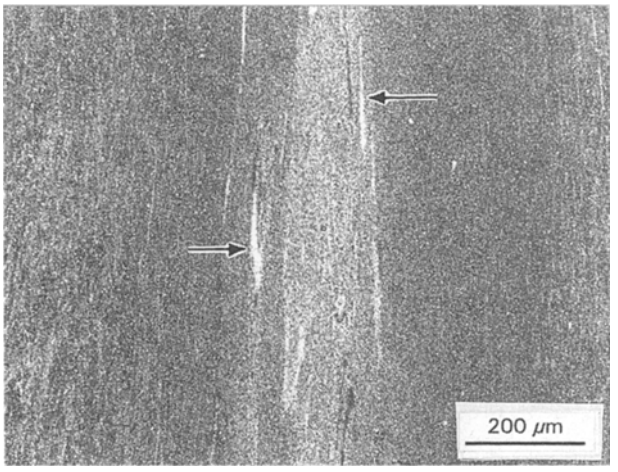

Figure 6 Optical micrograph of IHDZ near periphery of LAF weld. Arrows indicate featureless regions.

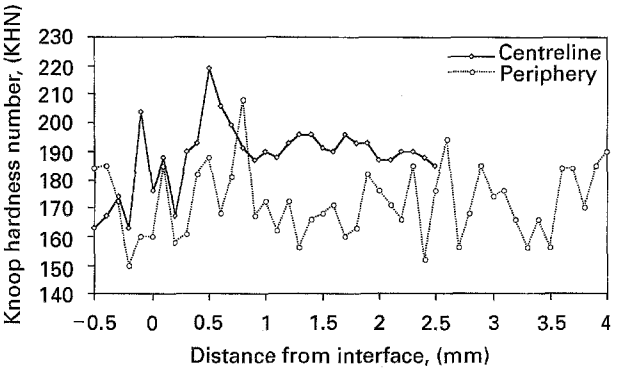

Figure 7 Microhardness vs distance data from locations shown previously in Fig. 4a and b.

The base material microhardness was between 155–190 KNH depending on the size and density of SiC and $Al_{13}(Fe,V)_3Si$ dispersoids encountered by the indenter during testing. Areas with a high density of dispersoids exhibited microhardness values on the order of 185–190 KHN, while the microhardness of regions with little SiC was approximately 155–160 KHN. Fig. 7 is a plot of microhardness versus distance from the weld interface for the HAF weld shown previously in Fig. 4(a, b). A smooth variation of microhardness with distance from the weld interface was not observed, however, no weakened zone of low hardness was identified. The average microhardness of the HDZs varied little from that of the base material spanning a range from approximately 150–200 KHN. The microhardness of the weld zone and base material averaged approximately 180 KHN, except in the featureless regions where the microhardness consistently averaged 140 KHN. Similar microhardness trends were observed in the LAF welds.

3.2.2. Tensile testing

A summary of the mechanical test data is presented in Table I. The average ultimate tensile strength (UTS) of the base material tested in the longitudinal orientation at room temperature was 563.1 MPa, and the average strain to failure was 4.37%. These values compare

TABLE I Tensile test data

Sample no.	UTS (MPa)	Joint efficiency (%)	Strain to failure (%)	Failure location
BM #1	562.4	NA	4.07	In Gauge Length
BM #2	560.3	NA	4.47	In Gauge Length
BM #3	566.7	NA	4.29	Outside Gauge
Avg (σ)	563.1 (3.2)		4.37 (0.34)	
HAF #1	523.3	92.9	3.12	OHDZ
HAF #2	505.0	89.6	2.21	OHDZ
Avg (σ)	514.1 (12.9)	91.3	2.66 (0.64)	
LAF #1	526.3	93.4	2.73	OHDZ
LAF #2	495.8	88.0	–	OHDZ
Avg (σ)	511.0 (21.6)	90.7	2.73	

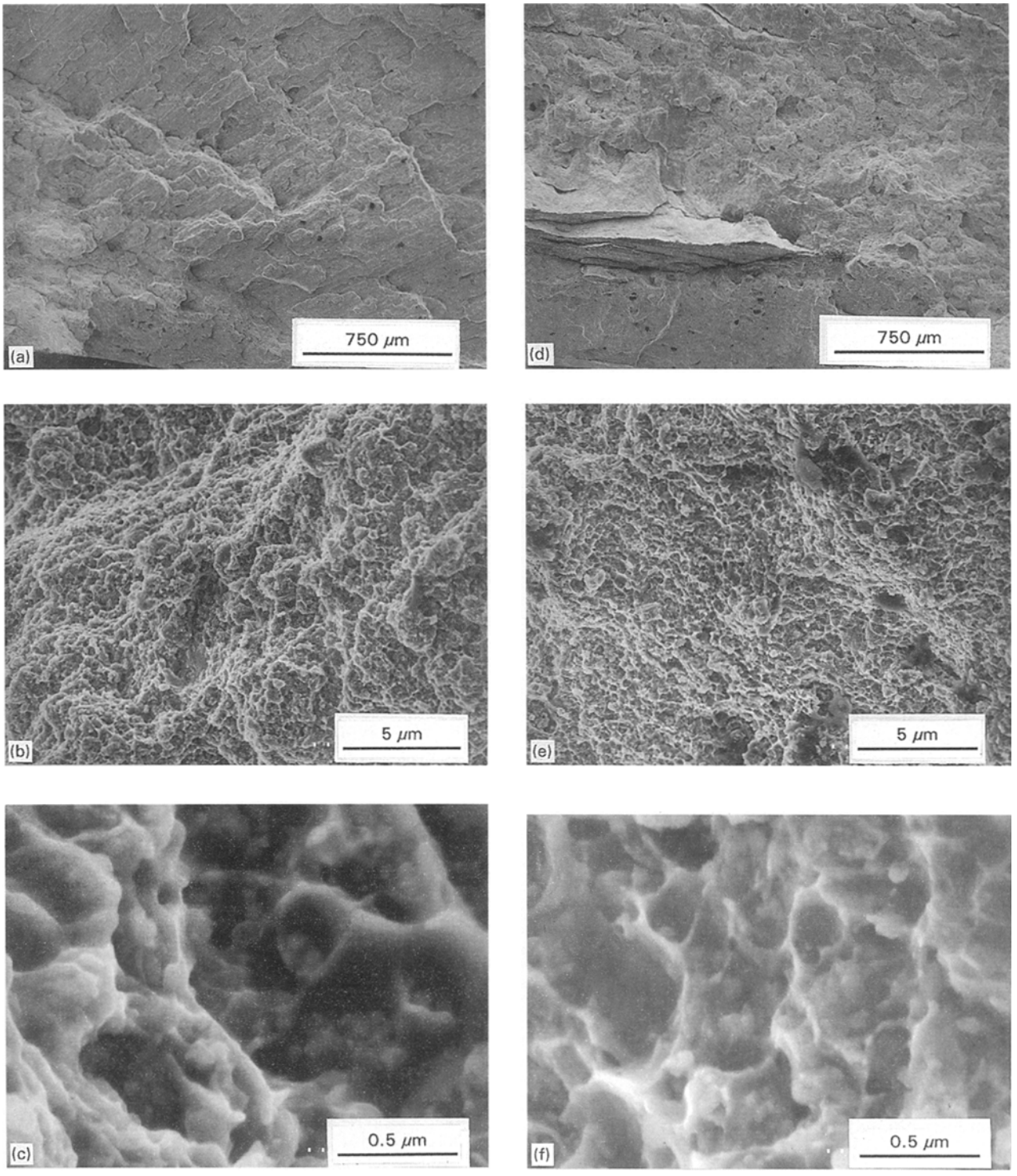

Figure 8 SEM fractographs of tensile specimens: (a–c) HAF weld; (d–f) base material.

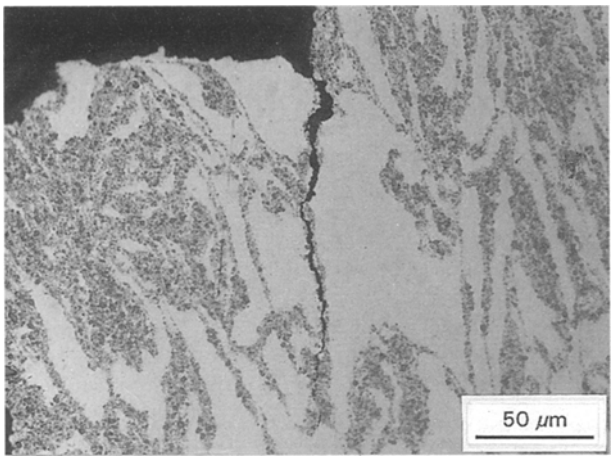

Figure 9 Optical micrograph of a section normal to the fracture surface of an LAF weld tensile specimen.

closely with those published previously [3]. The average UTS for the HAF welds was 514.1 MPa, and the average strain to failure was measured at 2.66%. For the LAF welds, the average UTS was 511.0 MPa and the strain to failure was 2.73%. The tensile strength joint efficiency, defined as the ratio of the weld UTS to that of the base material, was approximately 91% for both the LAF and HAF welds. Metallographic examination of the fractured samples indicated that failure occurred in the region of nearly equiaxed bands at the outer edge of the OHDZ for all of the welds tested.

3.2.3. Fractography

SEM micrographs of the fracture surfaces of the tensile samples for the base material and a HAF weld are shown in Fig. 8(a–f). Inspection of the low magnification fractograph from a HAF weld (a) revealed a preferred fracture orientation resulting from the deformation at this location of the OHDZ. A similar preferred orientation of fracture was not observed in the base material (d). At higher magnifications, the fracture surfaces of the 8009 matrix for both the HAF weld and the base material (b, c and e, f respectively) exhibited a dimpled appearance indicating a ductile failure, while the SiC fractured in a brittle fashion. The size, morphology and volume fraction of the particles in the centre of the dimples were consistent with those of the $Al_{13}(Fe, V)_3Si$ dispersoids reported previously [4]. The dark spots on the fracture surfaces were fractured SiC particles. Similar fracture surfaces were observed in the LAF welds.

Examination of the fractured tensile samples with optical microscopy revealed that failure occurred mainly through the 8009 matrix along a path of high SiC particle concentration. Fig. 9 is an optical micrograph of a polished section oriented normal to the fracture surface of a tensile specimen of a LAF weld. A secondary crack propagated through a region of dark contrast with a high density of SiC and was apparently blunted in the region of light contrast with no SiC. The ultimate fracture occurred along the main crack path. This behaviour is consistent with reports by other researchers in other Al/SiC composites in which clusters of SiC particles acted as initiation sites for fracture [32, 33]. The matrix adjacent to the SiC particles in the clusters experiences a higher level of constraint relative to other regions of the matrix resulting in a local loss in toughness.

4. Conclusions

The following conclusions may be drawn from the present study:

1. Inertia-drive friction welding (IFRW) has proven effective in producing high integrity, defect free joints in 8009/SiC/11_p.
2. The hot deformation experienced during welding produced a homogenized region along the bond line with a uniform distribution of SiC particles. No evidence of a chemical reaction between the SiC and the matrix was found in the welds, however, cracking of some of the larger SiC particles was observed in the base material as well as the IFR welds.
3. The Knoop microhardness of the base material varied considerably due to the microstructural variation of the matrix and the presence of SiC particles. The average microhardness of the different zones of the welds did not vary greatly from that of the base material, and no weld induced weak zones were observed.
4. Consistent with the microhardness results, the tensile joint efficiencies of the IFR welds exceeded 90 per cent.
5. The weld tensile specimens failed in the region at the outer edge of the heat-and-deformation affected zone for all of the welds tested.
6. The fracture surface of the 8009 matrix on tensile samples for both the base material and the IFR welds exhibited a dimpled appearance indicating a primarily ductile failure, while the SiC particles appeared to fracture in a brittle fashion.

Acknowledgements

The authors wish to thank AlliedSignal Inc. of Morristown, NJ for supplying the material used in this study. They also acknowledge Messrs. Tim Stotler and Aaron Crouse of EWI for their assistance in inertia-friction welding. Finally, the authors acknowledge support of this work by the Army Research Office under contract number DAAL03-92-G-0148 and the American Welding Society Foundation.

References

1. M. G. McKIMPSON, E. L. POHLENZ and S. R. THOMPSON, *JOM* **45** (1) (1993) 26.
2. American National Standard for Aluminum Metal Matrix Composite Materials (ANSI/ASC H35.5–1992).
3. M. S. ZEDALIS, J. D. BRYANT, P. S. GILMAN and S. K. DAS, *JOM* **43** (8) (1991) 29.
4. D. J. SKINNER, R. L. BYE, D RAYBOULD, A. M. BROWN and M. S. ZEDALIS, in Proceedings of Processing of Structural Metals by Rapid Solidification, Orlando, October 1986, edited by F. H. Froes and S. J. Savage (ASM International, Materials Park, OH, 1987) p. 291.

5. M. S. ZEDALIS, D RAYBOULD, D. J. SKINNER and S. K. DAS, in Proceedings of Processing of Structural Metals by Rapid Solidification, Orlando, October 1986, edited by F. H. Froes and S. J. Savage (ASM International, Materials Park, OH, 1987) p. 347.
6. H. H. KOO, S. KRISHNASWAMY and W. A. BAESLACK III, *Materials Characterization* **26** (1991) 123.
7. H. H. KOO and W. A. BAESLACK III, *Welding Journal Research Supplement* **71** (5) (1992) 147.
8. T. ISEKI, T. KAMEDA and T. MARUYAMA, *J. Mater. Sci.* **19** (1984) 1692.
9. K. K. WANG and P. NAGAPPAN, *Welding Journal Research Supplement* **49** (9) (1970) 419s.
10. K. K. WANG and W. LIN, *ibid* **53** (6) (1974) 233s.
11. G. E. DIETER, "Mechanical Metallurgy" (McGraw-Hill, New York, 1986).
12. W. A. BACKOFEN, in "Fracture in Engineering Materials" (ASM International, Materials Park, OH, 1964).
13. P. C. JOHNSON, B. A. STEIN and R. S. DAVIS, Report on Inertia Welding to the Caterpillar Tractor Company (Arthur D. Little, Inc., Cambridge, MA, 1966).
14. "Welding Handbook" – Eighth Edition (American Welding Society, Miami, 1991).
15. W. A. BAESLACK III and K. S. HAGEY, *Welding Journal Research Supplement* **67** (1988) 139 s.
16. K. H. HOU and W. A. BAESLACK III, *J. Mater. Sci.* **25** (1990) 2642.
17. M. J. COLA "Inertia-Friction Welding of Particulate-Reinforced Aluminum Matrix Composites", M.S. Thesis (The Ohio State University, 1992).
18. M. J. COLA and C. E. ALBRIGHT, in Proceedings of the 3rd International Conference on Trends in Welding Research, Gatlinburg, TN 1992, edited by S. A. David and J. M. Vitek (ASM International, Materials Park, OH, 1992) p. 1139.
19. O. T. MIDLING and Ø. GRONG, in Proceedings of the 3rd International Conference on Trends in Welding Research, Gatlinburg, TN 1992, edited by S. A. David and J. M. Vitek (ASM International, Materials Park, OH, 1992) p. 1147.
20. *Idem, Acta Metallurgica et Materialia* **42** (5) (1994) 1595.
21. *Idem, ibid* **42** (5) (1994) 1611.
22. L. E. SHOEMAKER, in Proceedings of the International Conference on Trends in Welding Research, Gatlinburg, TN 1986, edited by S. A. David (ASM International, Materials Park, OH, 1986) p. 371.
23. A. AMBROZIAK and R. LISON, *Welding Research Abroad* (12) (1993) 10.
24. Personal Communication, N. DeCristofaro, AlliedSignal Inc.
25. Personal Communication, M. S. Zedalis, AlliedSignal Inc.
26. G. T. VAN ROOYEN and W. A. BACKOFEN, *International Journal of Mechanical Science* **1** (1960) 1.
27. J. YANG, C. CADY, M. S. HU, F. ZOK, R. MEHRABIAN, and A. G. EVANS, *Acta Metallurgica et Materialia* **38** (12) (1990) 2613.
28. G. BAO, *ibid.* **40** (10) (1992) 2547.
29. Y. BRECHET, J. NEWELL, S. TAO and J. D. EMBURY, *Scripta Metallurgica et Materialia* **28** (1993) 47.
30. C. J. CHENG, *Welding Journal Research Supplement* **41** (12) (1962) 542s.
31. H. M. TENSI, W. WELZ and M. SCHWALM, *Aluminium* **58** (1958) 515.
32. Y. FLOM and R. J. ARSENAULT, *Acta Metallurgica et Materialia* **37** (9) (1989) 2413.
33. D. J. LLOYD, *ibid.* **39** (1) (1991) 59.

Received 19 September 1994
and accepted 17 October 1995